Proceedings of the Twelfth (2016) Pacific-Asia Offshore Mechanics Symposium
Gold Coast, Australia, October 4-7, 2016

ISBN 978–1 880653 98-2: ISSN 1946-004X

www.isope.org

Seabed Proximity Effects on the Wave-induced Hydrodynamic Forces on a Submarine Pipeline

Xiao-Fan Peng, Wen-Gang Qi & Fu-Ping Gao
Key Laboratory for Mechanics in Fluid Solid Coupling Systems, Institute of Mechanics, Chinese Academy of Sciences, Beijing, China

ABSTRACT

Most existing studies on the submarine pipeline hydrodynamics are either for the pipes above the seabed or for those buried in the seabed. In this study, the seabed proximity effects on the wave-induced hydrodynamics of the pipes with typical relative locations are investigated experimentally in a large fluid-structure-soil interaction flume. Experimental results indicate that when the pipe is above the seabed, the inertial coefficient C_M and upward lift coefficient C_{LA} increase with decreasing the gap-to-diameter ratios (e/D) for $e/D < 0.5$. With e/D decreasing from 1.0 to 0, the drag coefficient C_D and downward lift coefficient C_{LT} increase gradually and reach their peak values at $e/D \approx 0.1$, then decrease as the pipe further approaching the seabed. When the pipe is buried in the seabed ($e/D<0$), the effect of inertia on the in-line force gets weaken. The maximum values of the downward and upward lift forces happen approximately under the wave crest and wave trough, respectively. Moreover, the pore pressure oscillation amplitudes increase on the upper-half segment of the pipe and decrease on its lower-half segment in comparison with those at the same depths in the far-field.

KEY WORDS: submarine pipeline; pore pressure; hydrodynamic force; Morison equation; force coefficients; seabed proximity effects;

INTRODUCTION

While submarine pipelines approaching or penetrating into the seabed, the hydrodynamics can undergo significant changes in both magnitude and phase. To better understand the variations of hydrodynamic forces with the gap/embedment ratio is vital for the on-bottom stability design of a submarine pipeline.

For the fully exposed cylinders (unburied pipelines), Sarpkaya (1977) measured the in-line and transverse forces on the cylinders placed at various gaps from the bottom of the U-shaped water tunnel. In those experiments, the boundary layer thickness δ was relatively small (approximately $0.073D$, D is the pipe diameter) and the boundary layer effects were ignorable for the gap ratio e/D larger than about 0.1. Note that e denotes the gap ($e \geq 0$) or embedment ($e<0$) between the pipe bottom and the seabed surface. Flow visualization experiments showed that the gap blocks the flow and induces earlier separation over the top of the cylinder, which would increase both the in-line and the transverse forces. The experimental data showed that the seabed proximity effects cease to affect the flow and the force coefficients for $e/D>0.5$. Bryndum et al. (1992) investigated the hydrodynamic forces on a submarine pipeline resting on the seabed with no gap between the pipe and the impermeable rigid seabed. For the tests of typical hydrodynamic loads, three different methods were employed to analyze the hydrodynamic forces, including the least-squares-fit analysis based on Morison-type equations, the Fourier analysis, and the maximum force analysis. Xu et al. (2010) studied the bed form evolution around a submarine pipeline. Four regimes of the bed evolution behaviors were defined, i.e. no scour, scour without ripples, scour with small ripples and scour with large ripples. It was indicated that the wave forces on the pipe vary significantly in different bed form regimes.

For the pipeline partially-buried in the seabed ($-1<e/D<0$), the total force acting on the pipe is composed of two components, i.e., the dynamic pressure on the exposed segment in the water and the pore-pressure on the embedded segment in the seabed. Kumar et al. (2005) measured the wave pressure and uplift force due to random waves on a pipeline (resting on bed, half buried and fully-buried) in clayey soil. It was found that just burying the pipeline ($e/D=-1.0$) in clayey soil reduces the uplift force to less than 60% of the force experienced by a pipeline resting on the seabed ($e/D=0$) for consistency index I_c (I_c=(L.L-nmc)/(L.L-P.L), where L.L is the liquid limit; nmc is the natural moisture content; P.L is the plastic limit) of 0.33. Neelamani and Al-Banaa (2011) investigated the hydrodynamic forces on the pipeline due to random waves for different burial depths in four types of soil. It was indicated that the horizontal wave force reduces non-linearly with the increase of the relative burial depth of the pipeline, whereas the uplift force increases up to the half burial depth, beyond

which it reduces with the further increase of the burial depth. An et al. (2012) carried out an experimental investigation on the hydrodynamic forces acting on a partially-buried pipeline. The variation of normalized force coefficients with pipe embedment was compared with the results predicted by using reduction factors of hydrodynamic forces by DNV (2007). It is noted that the reduction factors given by DNV (2007) are not suitable for porous seabed conditions, especially for the case of fully-buried pipes.

For the pipeline fully-buried in the seabed, Magda (2000) investigated the wave-induced uplift force acting on a submarine pipeline buried in sandy seabed analytically and numerically. The results indicated that the perturbation pore pressure is important to the uplift force on the fully-buried pipeline. Sudhan et al. (2002) conducted an experimental investigation of wave-induced hydrodynamic forces on a pipeline buried in a permeable seabed. Their experimental data indicated that the wave induced pressures are significantly influenced by the wave period analyzed in terms of the scattering parameter ($\pi D/L$, L is the wave length).

As aforementioned, three typical relative locations between pipe and seabed can be categorized, i.e. the model pipe above the seabed, the partially-buried pipe, and the fully-buried pipe. Until now, the special research for the seabed proximity effects on the wave-induced hydrodynamic forces covering all the three typical pipe locations is scarce.

In this study, a series of physical modeling experiments were conducted to intensively investigate the seabed proximity effects on the wave-induced hydrodynamic forces on a submarine pipeline.

EXPERIMENTAL SET-UP

Testing facility

The experiments were carried out in a flow-structure-soil interaction flume (52 m long, 1 m wide and 1.5 m high) at the Institute of Mechanics, Chinese Academy of Sciences. Fig. 1(a) shows the schematic diagram of the experimental arrangement. Regular waves were simulated by a computer controlled piston-type wave generator located at the upstream end. A soil bed (5.0 m in length, 0.6 m in depth and 1.0 m in width) was laid in the middle section of the flume, whose mean particle diameter d_{50}=0.15mm, relative density D_r=0.62, the coefficient of permeability k_s =7.23x10^{-6} m/s, the geometric standard deviation σ_g=1.65, and the void ratio e_0=0.35.

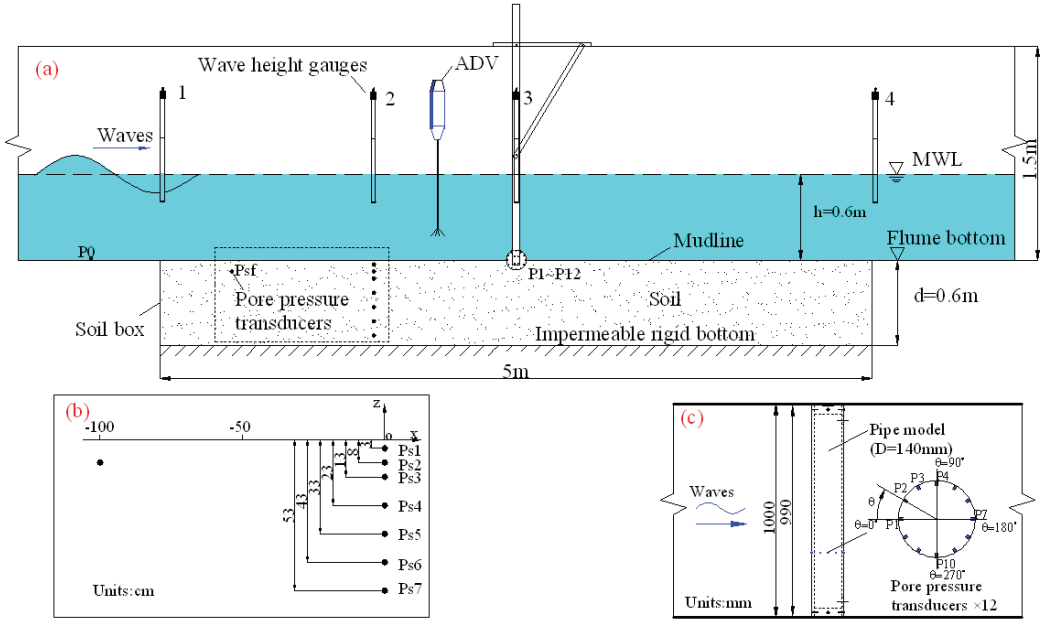

Fig .1 (a) Schematic diagram of the experimental system (front view); (b) Arrangement of the pore pressure transducers in the soil; (c) Detailed design of the model pipe (top view).

A model pipe of 990 mm length and 140 mm diameter was used in the tests. The pipe was laid perpendicular to the wave direction and fixed to the flume wall by a pair of supporting poles at its ends. Its location can be adjusted by the supporting frame for a certain value of the gap/embedment-to-diameter ratio. The pressure along the outer circumference of the pipe was measured with 12 miniature pore pressure transducers (see Fig. 1(c)). The hydrodynamic forces acting on the model pipe per unit length (F_H and F_L) are calculated by integrating the pressure along the circumference of the model pipe:

$$F_H \approx \sum_{i=1}^{12} \frac{\pi}{12} D(p_i - p_{i0}) \cos\alpha_i \quad (1)$$

$$F_L \approx -\sum_{i=1}^{12} \frac{\pi}{12} D(p_i - p_{i0}) \sin\alpha_i \quad (2)$$

where p_i and p_{i0} denote the total transient pressure and the static pressure measured by the ith pressure transducer, respectively; α_i is the position angle of the ith transducer.

As illustrated in Fig. 1(b), seven miniature pore pressure transducers (marked with Ps1, Ps2, … and Ps7) were placed at various depths in the soil; one miniature pressure transducer (P0) was mounted on the rigid floor. The transducers used were electrical resistance strain gauges. The strain gauges sense the resulting strain/deflection to give an output voltage proportional to the applied external pressure. A standard bridge amplifier was used to amplify the output to the required level. The transducer measuring capacity was 30 kPa and the measuring accuracy

was ±0.1%FS. Four wave height gauges were placed along the central line of the flume to measure the variation of wave heights at the edges of the soil bed, in the cross section of the pore pressure transducers in the soil bed and above the model pipe respectively. An Acoustic Doppler Velocimetry (ADV) was mounted to measure the velocity of the undisturbed wave-induced oscillatory flow at the axis of the model pipe for the cases of $e/D \geq 0$ and far-field velocity for the cases of $e/D<0$, respectively. The wave height, the velocity of wave-induced oscillatory flow, the pore-pressure around the pipe and in the soil bed were measured simultaneously via the NI USB-6255 Data Acquisition Card. The water depth (h) was kept constant (h = 0.6 m).

Test conditions

To study the effect of gap/embedment-to-diameter ratio on the transient hydrodynamic forces on the pipe, twelve burial-depths or gaps of the model pipe were adopted in the series of tests, including e/D=1.0, 0.5, 0.2, 0.1, 0.036, 0, -0.5, -1.0, -1.2, -1.4, -1.6, -2.0. As schematically illustrated in Fig. 2 (four specific cases), under the condition of $e/D>0$, the test pipe was located above the rigid floor to ignore the potential sediment transport; for $e/D<0$, the model pipe was embedded in the soil.

Regular waves were generated for each case. The wave parameters are summarized in Table 1, in which h is the water depth; H is the wave height; T is the wave period; U_m refers to the maximum velocity of the undisturbed wave-induced oscillatory flow at the level of pipe center for the cases of $e/D \geq 0$ and that at the level of $0.5D$ above the seabed for the cases of $e/D<0$; The KC, Re and β number are defined as U_mT/D, $U_m D/\nu$ and Re/KC respectively; ν is the kinetic viscosity of the water. The diameter of the submarine pipeline is approximately 0.5–1.5 m in the field scale, which makes the corresponding KC number with a typical range of 4–100. In the present test, the range of KC number is 4-10, which is considered as the inertia-dominated regime by Sumer and Fredsøe (1997). Test duration for each wave series was approximately 30 wave periods. Thus, after each wave series, the evolution of the seabed surface due to soil scour could be negligible. However, the sediment transport around the pipeline always occurs in real life. Ripples and scour around the pipeline can change the flow field and the hydrodynamic forces on the pipeline. The experimental results should be combined with the study on the sediment transport to apply to real life.

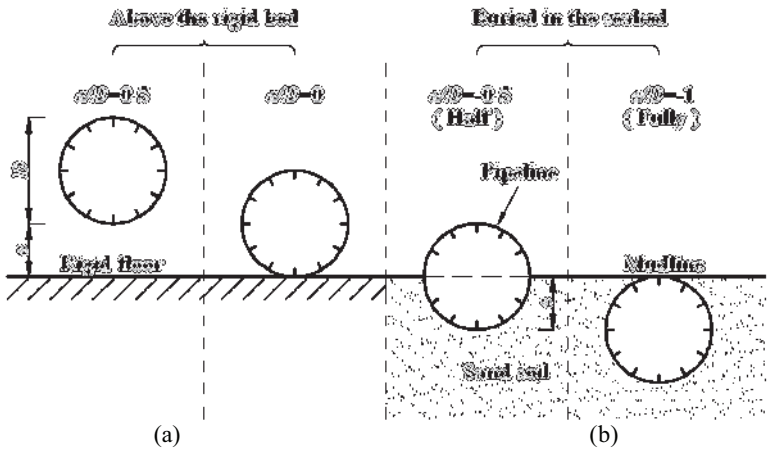

Fig. 2 Schematic diagram of typical locations of a near-bed pipeline: (a) above the seabed (e/D=0.5, 0); (b) half or fully buried in the seabed (e/D= -0.5, -1.0).

Table 1. Test conditions.

Run series number	h (m)	H (m)	T (s)	U_m (m/s)	KC	Re	β
1	0.6	0.20	2.2	0.28	4.35	3.40×10^4	7.82×10^3
2	0.6	0.20	2.4	0.33	5.71	4.09×10^4	7.17×10^3
3	0.6	0.20	2.6	0.35	6.58	4.35×10^4	6.62×10^3
4	0.6	0.22	2.2	0.32	5.10	3.99×10^4	7.82×10^3
5	0.6	0.22	2.4	0.38	6.47	4.64×10^4	7.17×10^3
6	0.6	0.22	2.6	0.38	7.12	4.71×10^4	6.62×10^3
7	0.6	0.24	2.2	0.36	5.73	4.48×10^4	7.82×10^3
8	0.6	0.24	2.4	0.38	6.54	4.69×10^4	7.17×10^3
9	0.6	0.24	2.6	0.43	7.94	5.26×10^4	6.62×10^3
10	0.6	0.26	2.2	0.40	6.32	4.94×10^4	7.82×10^3
11	0.6	0.26	2.4	0.39	6.75	4.84×10^4	7.17×10^3
12	0.6	0.26	2.6	0.46	8.55	5.66×10^4	6.62×10^3

TEST RESULTS

Time series of hydrodynamic forces

Fig. 3 gives the time development of the wave profiles, the velocities of the wave-induced oscillatory flow (despiked), the in-line (horizontal) forces and the lift (vertical) forces on the model pipe under the wave loading for various gap/embedment-to-diameter ratios. It is shown that both the wave and velocity profiles at wave troughs are flatter than those at wave crests, implying that the generated waves in the tests actually exhibited nonlinearity due to a relatively large wave steepness. For the pipes above the rigid floor (e/D=1.0, 0.2, 0), there exists a phase shift of approximately 90° between the velocity and the in-line force, indicating that the in-line force is dominated by the inertia. With the increase of the pipe embedment, the in-line force decreases and exhibits a smaller phase shift relative to the velocity. That is, the effect of inertia force on the pipe hydrodynamics becomes smaller with increasing burial depth.

Compared with the in-line (horizontal) force (F_H) (see Fig. 3(b)), the time development of the lift force (F_L) (see Fig. 3(c)) exhibits different trends for various gap/embedment-to-diameter ratios. For the pipes above the rigid floor (e/D=1.0, 0.2, 0), the lift force fluctuates twice in one wave period, which should be attributed to the twice vortex shedding in one wave period for $4<KC<10$. The lift force exhibits a different phase shift from the velocity of the wave-induced oscillatory flow. The fluctuation amplitude increases as the pipe approaching the bed. It is worth noting that under the condition of e/D=0, the lift force F_L is always upwards (i.e., away from the floor). This may be due to that the flow from the bottom of the model pipe is effectively blocked for the zero-gap condition, the maximum velocity and the minimum pressure always occur on the top of the pipe. For e/D=-0.5, -1.0, the lift force changes significantly in both magnitude and profile. The maximum value of F_L is under wave trough and the minimum value under wave crest.

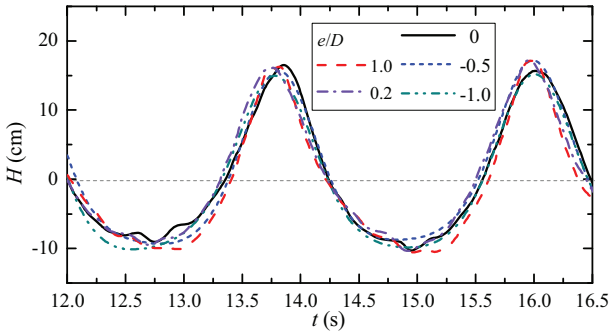

(a) Wave profile, H

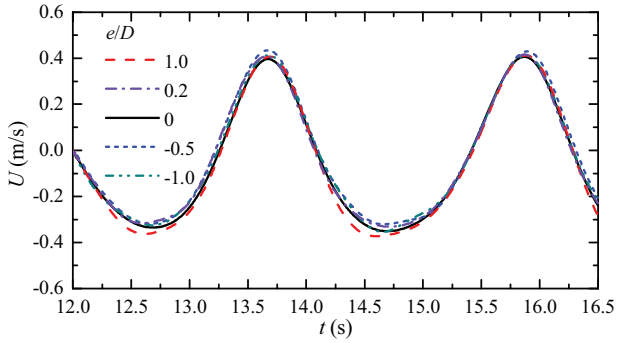

(b) Velocity of wave-induced oscillatory flow, U

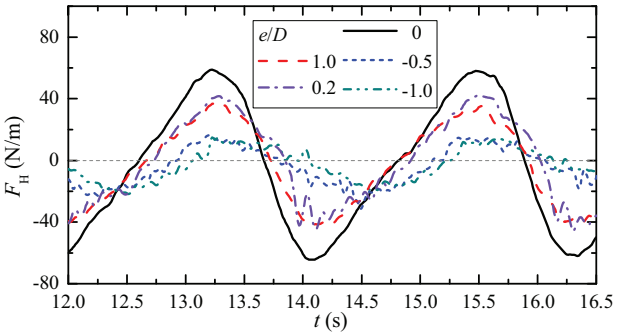

(c) In-line (Horizontal) force, F_H

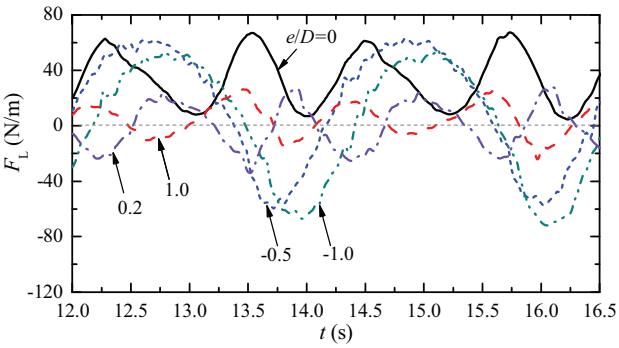

(d) Lift (Vertical) force, F_L

Fig. 3 Comparisons of velocities of the wave-induced oscillatory flow and hydrodynamic forces for various gap/embedment ratios (H=0.26 m, T=2.2 s).

Pore pressure response around the embedded pipe

Hydrodynamic forces may vary remarkably as the pipe is gradually penetrating into the seabed. Fig. 4 gives the distribution of the wave-induced pore-pressure along the circumference of the pipe located just under the wave crest and wave trough for e/D=-0.5, -1.0, -1.6. It can be identified that the pore pressure at the lower half section is smaller than that at the upper half section, which is attributed to the sheltering effect of the pipe. By integrating the (pore) pressures along the circumference

of the model pipe, the hydrodynamic forces can be calculated. As shown in Fig. 3(c), the time development of the lift forces changed significantly for various gap/embedment ratios (H=0.26 m, T=2.2 s). For the half buried (e/D=-0.5) and fully buried (e/D=-1.0), the maximum values of the downward and upward lift forces happen approximately under the wave crest and wave trough, respectively.

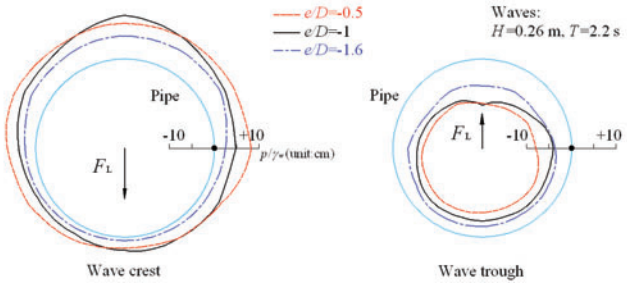

(a) (b)

Fig. 4 Distribution of wave-induced pore-pressure along the circumference of the pipe for e/D=-0.5, -1.0, -1.6 (H=0.26 m and T=2.2 s): (a) under the wave crest; (b) under the wave trough.

Fig. 5 shows the non-dimensional pore pressure amplitudes (p/p_0) around the model pipe for different burial depths. p_0 is the amplitude of pressure fluctuation at the seabed surface. The dash lines denote the non-dimensional pore pressure amplitudes at the same depth in the far-field soil bed (i.e., without the model pipe). For a given burial depth, the amplitudes of pore pressure oscillations are much larger on the upper half of the model pipe and smaller on the lower half of the model pipe than those at the same depths in the far-field. The pipe behaves like a wall boundary, which reflects the wave energy on the half side of the pipe and hinders the transfer of wave energy downwards the pipe. As the pipe burial depth increases, the amplitudes of pore pressure oscillations decrease accordingly.

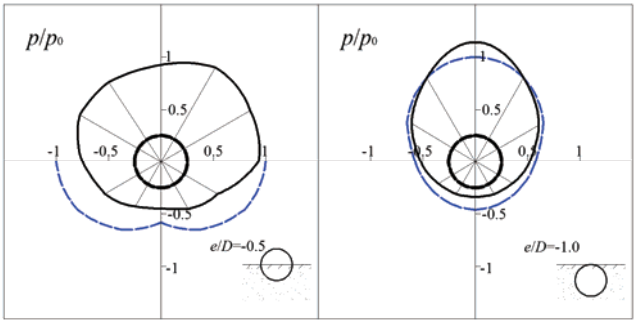

(a) (b)

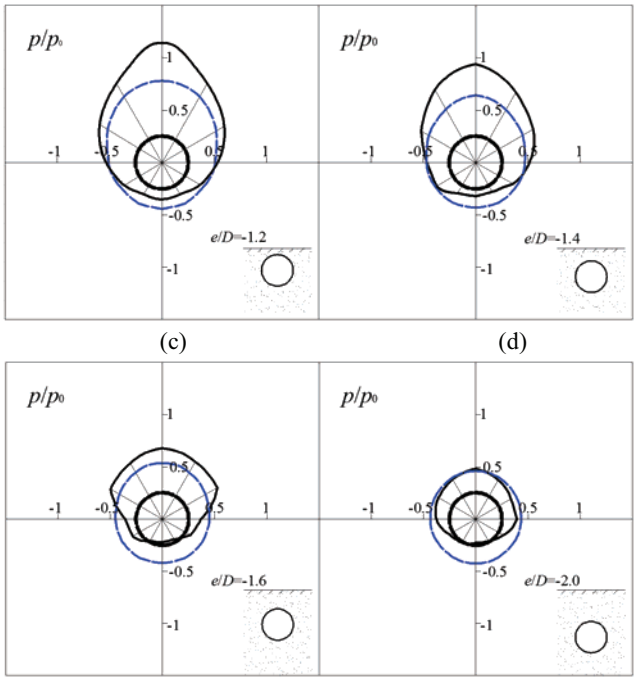

(c) (d)

(e) (f)

Fig. 5 Amplitudes of non-dimensional pore pressure along the circumference of the pipe (H=0.26 m and T=2.2 s): (a) e/D=-0.5; (b) e/D=-1.0; (c) e/D=-1.2; (d) e/D=-1.4; (e) e/D=-1.6; (f) e/D=-2.0.

Seabed proximity effects on hydrodynamic coefficients

The inertia and drag force coefficients (C_M and C_D) are used to account for wave-induced horizontal force per unit length on the pipe in Morison equation, i.e.

$$F_H = \frac{1}{2}\rho C_D D U|U| + \rho C_M A \dot{U} \tag{3}$$

where ρ is the mass density of fluid; D is the outer diameter of the model pipe; U is the undisturbed incident flow velocity at the center of the pipe. A is the cross sectional area of the pipe. As the values of $U(t)$ was measured by an ADV simultaneously at the location of Δx ahead to the pipe, a time shift of $\Delta t=\Delta x/U_p$ is applied to the measured velocity. Note that Δx is the distance between ADV and the center of the model pipe, and U_p is the propagation velocity of the wave. The time-shifted velocity $U(t+\Delta t)$ is thus adopted as the undisturbed flow velocity at the center of the model pipe. A method of least squares introduced by Sumer and Fredsøe (1997) is used to calculate C_M and C_D.

The lift coefficients C_{LA} (away from the seabed) and C_{LT} (toward the seabed) are used to account for the lift (vertical) forces per unit length on the pipe in Morison equations, i.e.

$$F_{LA} = \frac{1}{2}\rho C_{LA} D U_m^2 \tag{4}$$

$$F_{LT} = \frac{1}{2}\rho C_{LT} D U_m^2 \tag{5}$$

where F_{LA} is the maximum value of the lift force away from the seabed

and F_{LT} is that towards the seabed.

Fig. 6 gives a comparison between the force coefficients C_M, C_D and C_{LA} in the present experiments and the well-known curves for the wall-free conditions by Sarpkaya (1977). It is shown that the force coefficients C_M and C_D for e/D=1.0 in the present experiments are relatively smaller than the results by Sarpkaya (1977), which may attribute to the difference between the orbital flow in the present waves and the previous in-plane oscillatory flows. The force coefficients C_M, C_D and C_{LA} generally increase with decreasing e/D, indicating the seabed proximity effects are quite remarkable. It is noticed that the KC number in the present experiments is in the range of 4 ~ 10, which has been considered as the inertia-dominated regime (see Sumer and Fredsøe, 1997). That is, the drag force is relatively smaller that the inertia force. The distribution of drag coefficient is consequently more scattered compared with C_M and C_{LA}.

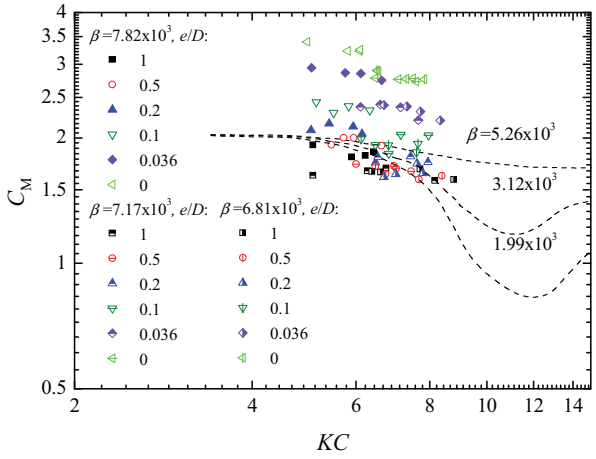

(a)

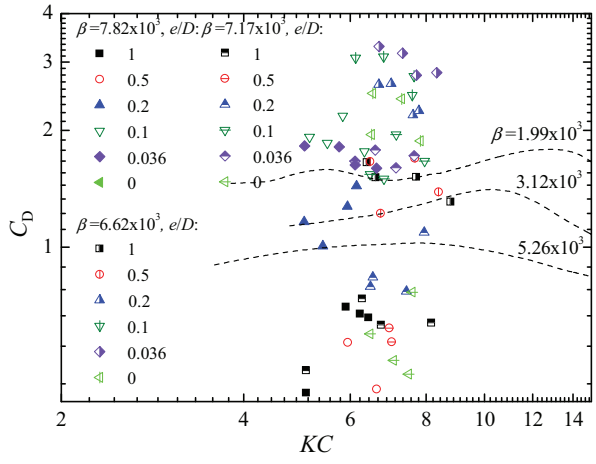

(b)

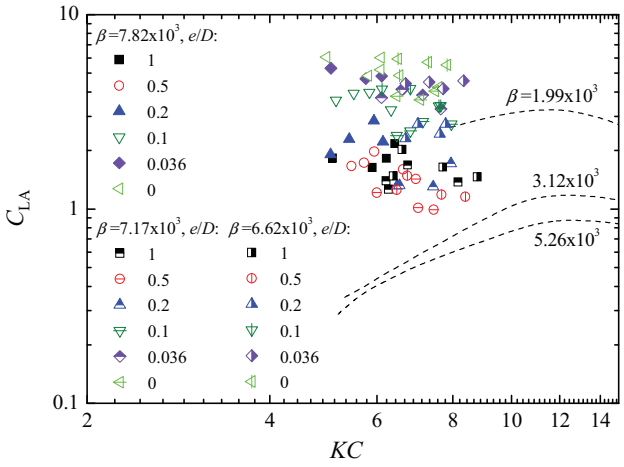

(c)

Fig. 6 Comparisons of C_M, C_D and C_{LA} between the present results and those by Sarpkaya (1977).

Fig. 7 presents the variations of the four hydrodynamic coefficients with the gap-to-diameter ratio in the present experiments ($e/D \geq 0$), which are in comparison with the potential-flow solution (e/D=0) by Yamamoto et al. (1974) and the modified potential-flow solution by Fredsøe and Hansen (1987). It is indicated that the inertia coefficients remain reasonably constant for e/D>0.5. Nevertheless, the inertia coefficient increases significantly with further decreasing e/D, indicating obvious seabed proximity effect. As KC decreases, the present C_M vs. e/D curves shift towards the predication with the potential theory by Yamamoto et al. (1974). For the small KC number, the flow separation and vortex shedding would be weaken, therefore the potential-flow theory predictions of C_M can be acceptable. Unlike the variations of C_M with e/D, as the model pipe approaching the seabed, the drag coefficient gradually increases and reaches a peak value at $e/D \approx 0.1$, then decreases instead as the pipe further approaching the seabed (e/D<0.1). As for the lift force, the present experimental results on C_{LA} present a similar trend as C_M; whereas C_{LT} shows a similar trend to C_D, and reaches its maximum at $e/D \approx 0.1$, which might be due to that the boundary layer effects could be ignored for e/D>0.1 (Sarpakaya, 1977). The experimental results of C_{LA} are much higher than the potential-flow results by Fredsøe and Hansen (1987), while match the theoretical prediction (e/D=0) by Yamamoto et al. (1974).

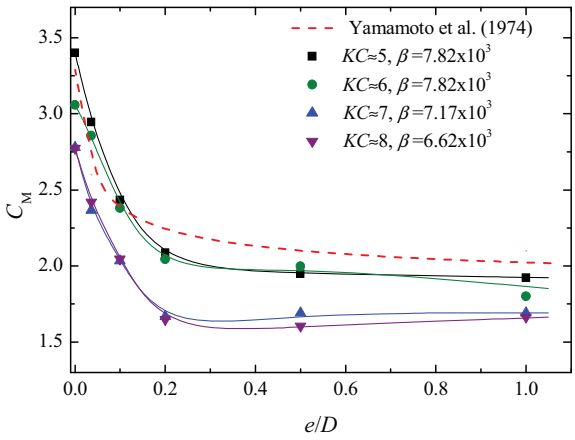

(a)

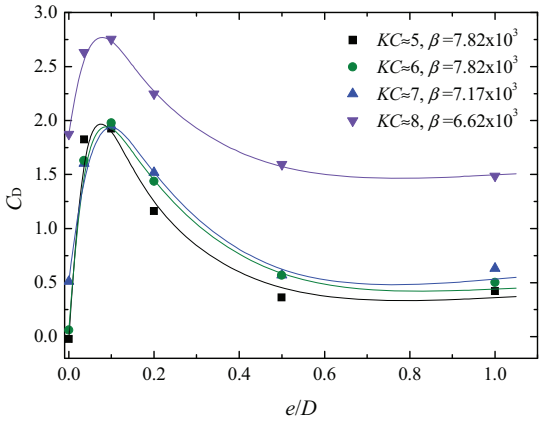

(b)

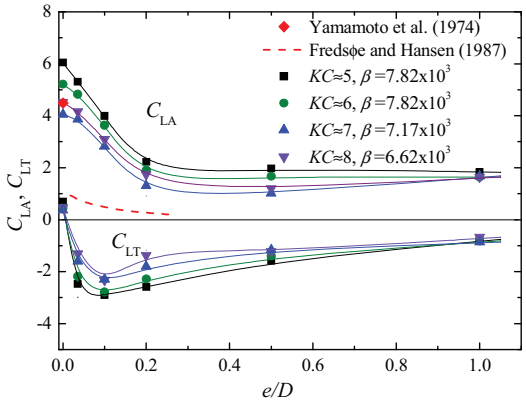

(c)

Fig. 7 Variations of C_M, C_D, C_{LA} and C_{LT} with e/D.

CONCLUSIONS

The seabed proximity effects on the wave-induced hydrodynamic forces on a submarine pipeline were investigated experimentally in a large flow-structure-soil interaction flume. Base on the experimental results, the following conclusions can be drawn:

1. For the KC number in the range of 4～10, the in-line hydrodynamic force on the pipeline is dominated by the inertia. With the increase of the pipe embedment, the inertia effect on the in-line hydrodynamics gets weaken. For the pipes above the seabed, the lift force fluctuates twice in one wave period, but exhibits a phase shift from the incident waves. When the pipeline is buried in the seabed, the lift force changes significantly in both magnitude and profile. The maximum values of the downward and upward lift forces happen approximately under the wave crest and wave trough, respectively.
2. When the pipeline is buried in the seabed, the amplitudes of pore pressure oscillation increase on the upper-half segment of the pipe, but decrease on the lower-half segment in comparison with those at the same depths in the far-field. As the burial depth increases, the amplitudes of pore pressure oscillation around the pipe circumference decrease accordingly.
3. When the pipeline is above the seabed, seabed proximity effects on the hydrodynamics are significant. Both C_M and C_{LA} increase with decreasing the gap-to-diameter ratio for e/D<0.5. C_D and C_{LT} increase gradually and reach their peak value at e/D≈0.1, then decrease as the pipe further approaching the seabed.

ACKNOWLEDGEMENTS

This work is financially supported by the National Natural Science Foundation of China (Grant Nos. 11232012; 11372319) and the Major State Basic Research Development Program of China (973 Program) (Grant No. 2014CB046204). Technical support from Mr. Fulin Zhang is greatly appreciated.

REFERENCES

An, H, Luo, C, Cheng, L, and White, D (2012). "A re-examination of the hydrodynamic forces acting on partially-buried submarine pipelines." *Proceedings of the 31st International Conference on Ocean, Offshore and Arctic Engineering*, 199-206.

Bryndum, MB, Jacobsen, V, and Tsahalis, DT (1992). "Hydrodynamic forces on pipelines: Model tests." *Journal of Offshore Mechanics and Arctic Engineering*, 114(4), 231-241.

Fredsøe, J, and Hansen, EA (1987). "Lift forces on pipelines in steady flow." *Journal of Waterway, Port, Coastal, and Ocean Engineering*, 113(2), 139-155.

Kumar, V, Neelamani, S, and Rao, SN (2005). "Wave interaction with a submarine pipeline in clayey soil due to random waves." *Ocean Engineering*, 32(13), 1517-1538.

Magda, W (2000). "Wave-induced cyclic pore-pressure perturbation effects in hydrodynamic uplift force acting on submarine pipeline buried in seabed sediments." *Coastal Engineering*, 39(2), 243-272.

Neelamani, S, and Al-Banaa, K (2011). "Wave force variation due to burial of submarine pipelines in uniformly graded and low hydraulic conductivity soil." *Applied Ocean Research*, 35, 47-55.

Sarpkaya, T (1977). "In-line and transverse forces on cylinders near a wall in oscillatory flow at high Reynolds numbers." *Proceedings of the Annual Offshore Technology Conference*, Houston.

Sudhan, CM, Sundar, V, and Rao, SN (2002). "Wave induced forces around buried pipelines." *Ocean Engineering*, 29(5), 533-544.

Sumer, BM, and Fredsøe, J (1997). *Hydrodynamics Around Cylindrical Structures.* World Scientific.

Det Norske Veritas (2007). *On-Bottom Stability Design of Submarine Pipelines*. Oslo, Norway. DNV-RPF109.

Xu, J, Li, G, and Dong, P (2010). "Bedform evolution around a submarine pipeline and its effects on wave-induced forces under regular waves." *Ocean Engineering*, 37(2): 304-313.

Yamamoto, T, Nath, JH, and Slotta, LS (1974). "Wave forces on cylinders near plane boundary." *Journal of the Waterways, Harbors and Coastal Engineering Division*, *ASCE*, 100(4), 345-359.